Generation of high-resolution surface temperature distributions

Anton A. Darhuber and Sandra M. Troian[a)]
Microfluidic Research and Engineering Laboratory, Department of Chemical Engineering, Princeton University, Princeton, New Jersey 08544

Sigurd Wagner
Department of Electrical Engineering, Princeton University, Princeton, New Jersey 08544

(Received 16 October 2001; accepted for publication 8 February 2002)

We have performed numerical calculations to study the generation of arbitrary temperature profiles with high spatial resolution on the surface of a solid. The characteristics of steady-state distributions and time-dependent heating and cooling cycles are examined, as well as their dependence on material properties and device geometry. Ideally, low-power consumption and fast response times are desirable. The simulations show that the achievable spatial resolution is on the order of the substrate thickness and that the response time t_+ depends on the width of the individual heating elements. Moreover, the rise time t_+ can be significantly shortened by deposition of a thermal insulation layer, which also reduces the power consumption and increases lateral resolution.
 [DOI: 10.1063/1.1465506]

I. INTRODUCTION

The recent trend towards miniaturization in biotechnology and material science has introduced many applications which require localized temperature distributions with high spatial resolution. Arrays of micromachined hot plates have been used to investigate the temperature dependence of desorption kinetics and growth of SnO_2 films.[1,2] Micro-hot plates have also been used to fabricate SnO_2 integrated gas sensors.[3,4] Akahori *et al.* and Kajiyama, Murakawa, and Miyahara have fabricated miniaturized device arrays for electronically addressable DNA replication.[5,6] Sammarco and Burns used polysilicon heaters for thermocapillary pumping of minute liquid volumes through an enclosed microchannel.[7] They also performed two-dimensional heat transfer simulations to study design options and the device performance under steady-state conditions.[8] For most of these applications, the relevant parameters are the time constants, the temperature uniformity over a heating element, cross talk within the array, and the power required to maintain a given temperature difference.

We have been exploring thermocapillary flow as an alternative method for microfluidic actuation wherein liquid migration is directed along the surface of a chemically micropatterned chip. Since the surface tension of liquids typically decreases monotonically with increasing temperature, small quantities of liquids can be moved along a solid substrate bearing an inhomogeneous temperature distribution.[9–12] Thermocapillary transport is due to the shear stress induced at the air–liquid interface by the applied thermal gradient. The flow direction is from warmer to cooler regions on the substrate. By confining the liquid to a lithographically defined network of hydrophilic channels,[13] a pixelated surface temperature profile can then be used to route liquids along arbitrary pathways with electronic control over the rate, direction, and timing of the flow. This application requires temperature fields with high temporal and positional resolution, which define the minimum time and length scale for the microfluidic flow.

In this article, we present numerical simulations addressing the achievable spatial resolution and smoothness of surface temperature distributions, the response times for heating and cooling, and the power consumption for electrical heating. Moreover, we investigate the feasibility of a pulsed operation mode, where only one resistor in an array is heated at any given time, versus operation in continuous mode where all resistors are heated simultaneously. The simulations, performed with realistic device layouts and material parameters, are intended to assist in their design and optimization.

II. DEVICE LAYOUT AND MATERIALS

The purpose of this study is to control the surface temperature of a solid electronically with high spatial and temporal resolution with minimal thermal coupling between neighboring pixels. Consequently, the lateral heat transfer between pixels must be reduced as much as possible. This is accomplished by introducing a heat sink beneath the substrate which directs the majority of the thermal flux normal to the surface. Moreover, the temperature-controlled heat sink provides a constant operating temperature for the substrate and prevents the device from heating up continuously. For this reason it is advantageous to keep the substrate thickness to a minimum; however, this increases the power consumption required to maintain a given vertical temperature difference. This consumption can be reduced by interposing a polymeric insulation layer with low thermal conductivity between the heaters and the substrate.

Figure 1(a) shows a cross-sectional sketch of the proposed device for a sample including three heaters. The heater array consists of microfabricated thin-film resistors deposited

[a)]Author to whom correspondence should be addressed; electronic mail: stroian@princeton.edu

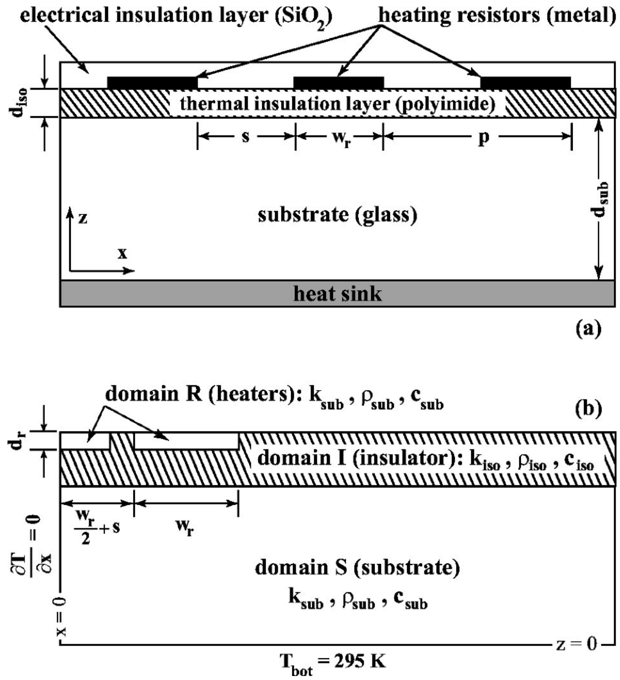

FIG. 1. (a) Cross-sectional diagram of the device layout. The black rectangles represent heating resistors with a typical thickness of 100 nm, widths w_r ranging from 10 to 1000 μm, and a lateral period p spanning 10–1000 μm. The thickness of the substrate d_{sub} ranges from 0.1 to 1 mm, while that of the thermal insulation layer d_{iso} ranges from 10 to 100 μm. (b) Diagram corresponding to the computational model which consists of three domains—S (substrate), I (insulation layer) and R (heating resistors) - characterized by material properties k, ρ, and c_p. The exterior boundary conditions are such that the bottom plane $z=0$ is held at constant temperature T_{bot}, the left boundary $x=0$ is a plane of symmetry, i.e., $\partial T/\partial x=0$, and the right and top surfaces are subject to radiative and convective heat transfer.

on an electrically insulating substrate like glass or polyimide. The metal heaters are coated with a 600 nm layer of SiO_2 using plasma-enhanced chemical-vapor deposition (PECVD) for electrical insulation. This coating is then hydrophobized and lithographically patterned for liquid confinement.[13] The metal resistors, which are sketched black in Fig. 1(a), are made by electron-beam evaporation of Ti and have a typical thickness of 100 nm. The resistors are coated with an 80 nm Au layer to minimize power dissipation in the contacts and leads. Since the electrical resistivity of Au is about 19 times lower than that of Ti, the contacts do not significantly contribute to the total resistance R.

The surface temperature distribution can be monitored by measuring the resistance change with temperature, $\Delta R=\beta R\Delta T$, where β is the thermal coefficient of the electrical resistivity. Typical values of β for metals range from 0.002 to 0.004 K^{-1}. Suitable materials for the device layers are glass (Corning 1737F) for the substrate, polyimide (Durimide, Arch Chemicals) for the underlying thermal insulation, and PECVD SiO_2 for the electrical insulation layer. The thermal properties of these materials are listed in Table I.

III. HEAT TRANSFER CALCULATIONS

We performed two-dimensional stationary and time-dependent heat transfer simulations for the cross-sectional geometry sketched in Fig. 1(b). The equation governing the temporal evolution of the temperature field $T(x,z)$ is

$$\nabla\cdot(k\nabla T)+\dot{q}=\rho c_p\frac{\partial T}{\partial t}, \qquad (1)$$

where k is the thermal conductivity, $\dot{q}$ the thermal power generation density, ρ the density, and c_p the specific heat capacity of the three computational domains defined in Fig. 1(b). Continuity of temperature is assumed at all interior domain boundaries. For these calculations, the substrate length was chosen sufficiently large to exclude end effects.

The boundary conditions corresponding to the exterior domains were chosen as follows: mirror symmetry about $x=0$, which enforces $\partial T/\partial x=0$; a constant ambient temperature $T_{bot}=295$ K at the substrate bottom $z=0$; and convective $h(T-T_{amb})$ and radiative losses $\epsilon\sigma(T^4-T_{amb}^4)$ across the top and right boundaries. Throughout the simulations, the convective heat transfer coefficient h was held fixed at 7.5 W/m^2K,[14,15] and the emissivity was chosen to be $\epsilon=0.9$. The Stefan–Boltzmann constant σ is 5.669×10^{-8} $Wm^{-2}K^{-4}$.

The Nusselt number,[15] which compares the rate of heat loss into the air by convection to conduction, is estimated to be $\mathrm{Nu}=hL/k_{air}\approx14$, where $L\approx5$ cm is the length of the device. Conductive losses into the air can, therefore, be ignored. Since the relevant surface temperatures for the proposed device range from room temperature to about 45 °C, the radiative flux can be comparable to convective fluxes. Although these are small, they are included in the computations. The dominant mode of heat transfer is conduction from the surface to the heat sink since the Biot number, which

TABLE I. Material constants for the substrate, insulation and resistor material and relevant liquids. Entries denote thermal conductivity k, density ρ, heat capacity c_p, and thermal coefficient of electrical resistivity β. The values of β for Ti and Au depend strongly on the concentration of impurities in the metal.

Material	k (W/K m)	ρ (kg/m^3)	c_p (J/kg K)	β (K^{-1})	Ref.
1737F	1.0	2540	(800)	⋯	21
Polyim.	0.1–0.15	1390–1590	1090	⋯	22–24
SiO_2	1.1–1.4	2000–2270	750–1000	⋯	25,26
Ti	15–22	4540	520	$\leq$0.0038	25,27
Au	291–318	19300	128	$\leq$0.004	25,27
PDMS	0.14–0.16	900–980	1550	⋯	28
Glycerol	0.285	1260	2416	⋯	25
Water	0.6	1000	4180	⋯	25

reflects the ratio of heat transfer by conduction through the solid to convection into the air, is estimated to be Bi $=hd_{\rm sub}/k_{\rm sub}\approx 0.0075$.

The numerical simulations were performed with the finite-element analysis program FEMLAB 2.1. Since the thickness of the metal resistors is typically 100 nm, whereas the substrate thickness $d_{\rm sub}$ is on the order of 1 mm, numerical difficulties can arise from the vast difference in length scales. The experimental device layout was, therefore, modeled according to the sketch in Fig. 1(b) in which the electrical power is dissipated in a layer with the thermal properties of the substrate and a thickness d_r of a few microns. This simplification leads to a slight underestimate in the surface temperature rise by about 3.5% for $d_r=9$ μm with proportionally less error for smaller values of d_r. Typical values of d_r used in the simulations were 3–5 μm.

A. Stationary temperature profiles

In this section we compute the achievable spatial resolution for stationary temperature profiles including its dependence on substrate thickness $d_{\rm sub}$ and resistor width w_r. We show how the rise in surface temperature can be controlled by the geometric device parameters as well as the interposition of a polymeric thermal insulation layer.

1. Single activated resistor

Since Eq. (1) is linear and the (nonlinear) radiative heat losses very small, the solution for a multitude of heat sources is essentially a linear superposition of solutions corresponding to individual heat sources. We first consider the case of a single activated resistor element centered at $x=0$, which is continuously heated.

Figure 2(a) shows the surface temperature increase $\Delta T(x,z=d_{\rm sub})$ in the absence of an insulating layer for a heater width $w_r=1000$ μm and a substrate thickness $d_{\rm sub}$ ranging from 50 to 1000 μm. The electrical power input $P=\dot{q}(w_r d_r l_r)$ was kept constant at 0.1 W, where resistor length l_r in the y direction was assumed to be 1 cm in all calculations. For small values of $d_{\rm sub}$, the thermal profile across the width of the heater is essentially flat, whereas for large values of $d_{\rm sub}$ it varies significantly, with the temperature maximum centered above the heating element.

The maximum temperature difference $\Delta T_{\rm max}$ between the top surface and the heat sink as a function of the substrate thickness is plotted in Fig. 2(b). For large values of $w_r/d_{\rm sub}$, the geometry resembles a conducting plate heated from above. In this limit, $\Delta T=d_{\rm sub}P/(w_r l_r k_{\rm sub})$ [solid lines in Fig. 2(b)]. $\Delta T_{\rm max}$ increases with decreasing resistor width since the thermal power density $\dot{q}$ increases for constant P. In the limit $w_r/d_{\rm sub}\rightarrow 0$ the geometry resembles a point source and the thickness dependence of $\Delta T_{\rm max}$ becomes weaker (approximately logarithmic) as lateral heat diffusion becomes more important.[16] The curves shown in Fig. 2(b) collapse onto a single curve if plotted as a function of the ratio $d_{\rm sub}/w_r$. This follows because in steady state Eq. (1) is invariant under a global rescaling of the in-plane coordinates and dimensions with P/l_r kept constant: $(x,z)\rightarrow(ax,az)$ and $(w_r,d_{\rm sub})\rightarrow(aw_r,ad_{\rm sub})$. Further simulations (not shown)

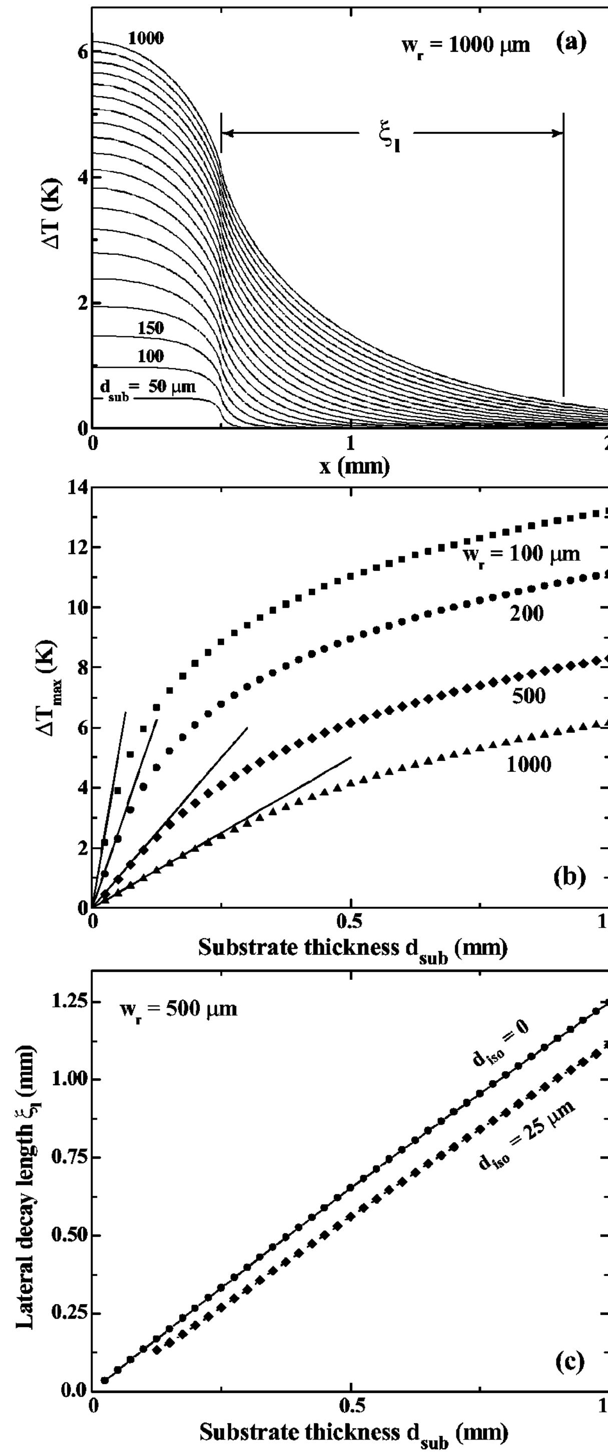

FIG. 2. (a) Surface temperature $\Delta T=T(x,z=d_{\rm sub})-T_{\rm bot}$ for a single activated heater and values of $d_{\rm sub}$ ranging from 50 to 1000 μm, $w_r=1000$ μm, $k_{\rm sub}=1$ W/mK, and $P=0.1$ W. The temperature profile is symmetric about the center of the heating element located at $x=0$. (b) Temperature difference $\Delta T_{\rm max}$ between top and bottom surface as a function of $d_{\rm sub}$ for different heater dimensions and $d_{\rm iso}=0$. (c) Lateral decay length ξ_l as a function of $d_{\rm sub}$ for a single activated 500-μm-wide resistor on a glass substrate. The dashed line corresponds to a 500-μm-wide heater on an additional 25-μm-thick polyimide insulation layer, which reduces ξ_l by about 9%.

reveal that $\Delta T_{\rm max}$ is proportional to P and inversely proportional to $k_{\rm sub}$, which can also easily be deduced from Eq. (1).

In Fig. 2(c) is shown the lateral decay length ξ_l of the temperature profile, defined as the length over which the

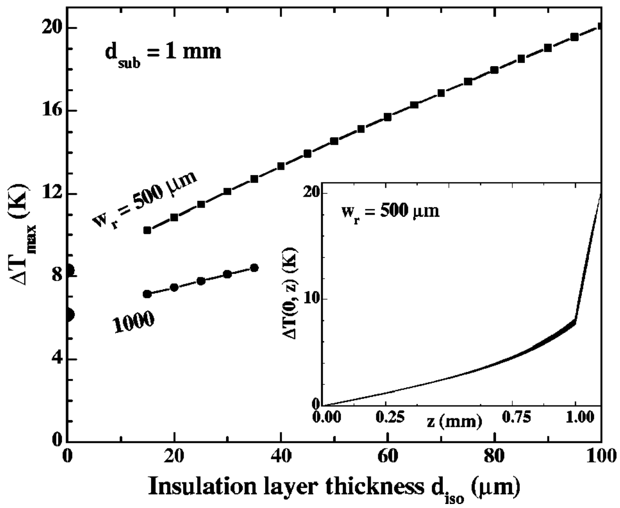

FIG. 3. Temperature difference $\Delta T_{\max}$ as a function of the thickness of the insulation layer d_{iso} for $d_{\text{sub}}=1$ mm and two values of w_r. The two black dots for $d_{\text{iso}}=0$ are extracted from Fig. 2(b). Inset: Vertical temperature profiles $T(x=0,z)$ for d_{iso} ranging from 15 to 100 μm. The temperature profile within the glass substrate is almost unaffected by the value of d_{iso}.

temperature $\Delta T(x)$ decreases by 90% of $\Delta T(x=w_r/2)$. The decay length increases with increasing values of d_{sub}, thus diminishing positional resolution. As shown in Fig. 2(c), ξ_l is almost linearly proportional to d_{sub}. Further simulations have shown that ξ_l depends only weakly on w_r and is practically independent of k_{sub}.

In order to reduce the power required to maintain a desired temperature difference, a polymeric insulation layer with low thermal conductivity can be interposed between the heater element and the glass substrate. Polyimide has a typical conductivity of $k_{\text{iso}}=0.15$ W/m K and can be spin-coated onto the substrate or applied as a foil prior to the evaporation of the metal resistors. If a 25-μm-thick polymeric layer is coated onto the glass substrate underneath the heating resistors, the lateral decay length is slightly smaller [dashed line in Fig. 2(c)], since the insulation layer decreases the lateral heat flux. Conversely, it is disadvantageous to place the insulation layer at the bottom of the substrate, since this increases ξ_l and decreases the achievable resolution significantly. In Fig. 3 we present the temperature difference $\Delta T_{\max}$ as a function of the thickness of the insulation layer for 500- and 1000-μm-wide heaters and a 1-mm-thick glass substrate.

Since the temperature gradient across such a thin insulation layer is essentially constant, $\Delta T_{\max}$ increases rather linearly with d_{iso}. The two data points located at $d_{\text{iso}}=0$ are taken from Fig. 2(b). The inset of Fig. 3 shows $\Delta T(0,z)$ corresponding to 18 values of d_{iso}. Each curve terminates at a different value of z—the thicker the insulation layer, the further extends the temperature profile but the slopes are almost unaffected. The slopes of the temperature profiles remain insensitive to d_{iso} provided $d_{\text{iso}} \ll d_{\text{sub}}$.

2. One-dimensional array of resistors

The decay length ξ_l determines the lateral overlap of the temperature distributions which can introduce "cross talk" between neighboring heating elements in a one-dimensional array. In certain microfluidic applications, it is desirable to enforce linear temperature distributions.[17] Ideally, the temperature of a particular heating element is strictly determined by the electrical power P dissipated in that resistor. If the temperature of the heating resistor is influenced by neighboring heaters, the proper set-point P will also depend on the power values of adjacent heaters. Therefore, if the lateral decay length is too large, real-time calculations of overlapping temperature distributions would be required in order to control the surface temperature, in much the same fashion as proximity effect compensations are needed in electron-beam lithography.[18]

Figure 4(a) shows the temperature distribution of a linear array of ten resistors distributed in the same way as sketched in Fig. 1(b) for three different heater widths $w_r=100$, 400, and 800 μm. The power P supplied to the individual resistors is set to decrease linearly from 0.1 to 0.01 W from the left- to the rightmost one. Undulations in the temperature profile for 100-μm-wide heaters are due to overlapping contributions from individual heating elements since $\xi_l \gg w_r$ and $\xi_l \gg s$. As the heater width increases, the maximum temperature is reduced since $\dot{q}$ decreases for constant P; however, the temperature profile becomes more linear. The inset in Fig. 4(a) shows the influence of spacing s between the resistors. This spacing should be smaller than about 20 μm, to help enforce a smooth and monotonic variation in temperature.

Figure 4(b) shows the temperature profile for the same linear array as in Fig. 4(a) except that no power is supplied to the fourth resistor. For a width of 800 μm, the temperature at the position of the fourth resistor drops only to 45% of the corresponding on value. At twice the width $w_r=1600$ μm, the temperature drops to 22% of the ON value. This effect is again due to the lateral coupling of neighboring heating elements.

B. Dynamic response—transient temperature profiles

For device operation, it is not only the steady state but also the dynamic response and corresponding time constants that are important. If the sample is initially at constant temperature T_{bot} and one or more heating elements have been activated, the temperature profile becomes stationary after a finite rise time t_+. Likewise, if a heating element is switched off, the temperature decreases with a characteristic decay time t_-. The decay time t_- is essentially equal to the rise time t_+ if the power to the resistor is switched on and off instantaneously. In this section we study the influence of the geometry and the material parameters on the time response of a single activated heating element within an array. Rise and decay times are defined as the time intervals over which temperature $T-T_{\text{bot}}$ changes by 63.21% of $\Delta T_\infty \equiv T(t\to\infty) - T_{\text{bot}}$.

Figure 5(a) shows rise times t_+ for a 1-mm-thick glass substrate as a function of the heater width w_r with and without a 25-μm-thick insulating layer. Only a single resistor is heated. The inset shows the time evolutions of the surface temperature

$$\Delta T_{\max}(t) \equiv T(x=0,z=d_{\text{sub}}+d_{\text{iso}},t) - T_{\text{bot}}, \quad (2)$$

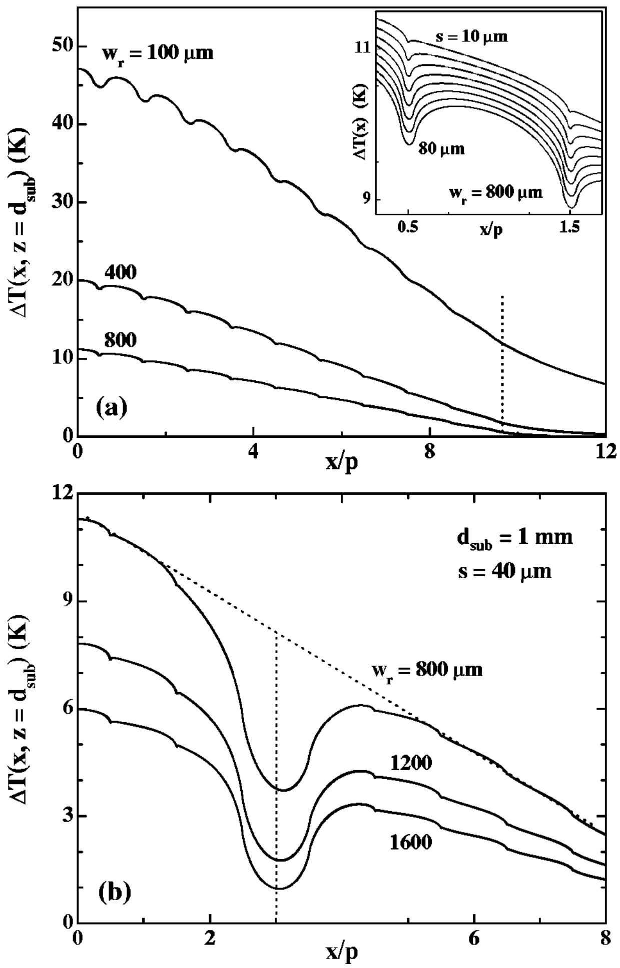

FIG. 4. (a) Surface temperature profiles for three different arrays of ten resistors each powered by an input P distributed linearly from 0.1 to 0.01 W across the array. The x coordinate is scaled by the lateral array period p, which is the sum of the resistor width w_r and the spacing s between neighboring heaters. The dashed line denotes the rightmost end of the heater arrays. The values of s and d_{sub} were kept constant at 40 μm and 1 mm. The insulation layer thickness d_{iso} was set to zero. Inset: Surface temperature profiles for w_r = 800 μm and s ranging from 10 to 80 μm. (b) Surface temperature profiles for three values of w_r and the same geometry and linear power distribution as in (a) except that the fourth resistor is inactive. The temperature at the position of the fourth resistor drops to 45%, 33%, and 22% of the ON value for w_r=800, 1200, and 1600 μm.

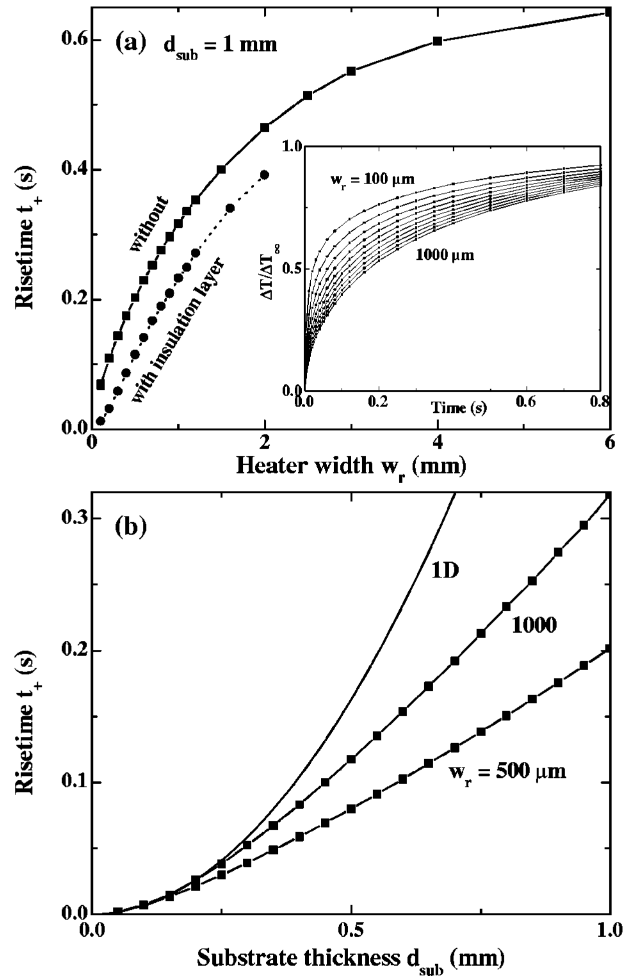

FIG. 5. (a) Rise times t_+ as a function of the heater width w_r for a 1-mm-thick glass substrate with (full line) and without (dashed line) a 25-μm-thick insulation layer. Inset: Time evolution of the surface temperature in the center of the heater for w_r ranging from 100 to 1000 μm. (b) t_+ as a function of the substrate thickness for w_r=500 and 1000 μm and d_{iso}=0.

in the center of the heater normalized by its asymptotic value

$$\Delta T_\infty = T(0, d_{sub} + d_{iso}, t \to \infty) - T_{bot}, \tag{3}$$

for w_r ranging from 100 to 1000 μm. For increasing values of w_r/d_{sub}, the geometry approaches that of one-dimensional heat transfer through a two-layer system and t_+ saturates at the corresponding value.

Interestingly, the rise time is *smaller* when the insulation layer is present, despite the decrease in overall thermal diffusivity α and increase in total thickness. For a sample with homogeneous thermal properties, the rise time is proportional to the square of the thickness and inversely proportional to the thermal diffusivity $\alpha = k/(\rho c_p)$.[14] The reason for the decrease in t_+ is the large difference between the thermal conductivities of the insulation layer and the substrate. In the following we illustrate this effect in the parallel-plate limit and derive an approximate expression for t_+ for the composite two-layer geometry. In this limit, the steady-state temperature difference between the top and bottom surfaces is given by

$$\Delta T_\infty = \left(\frac{d_{iso}}{k_{iso}} + \frac{d_{sub}}{k_{sub}} \right) \frac{P}{w_r l_r} \equiv \Delta T_{iso} + \Delta T_{sub}. \tag{4}$$

As Fig. 3 shows, even a comparatively thin insulation layer can make a significant contribution to ΔT_∞ since $k_{iso} \ll k_{sub}$. As the power to the resistor is switched on, the heat front first traverses the thin insulation layer with a corresponding time constant $t_{+iso} \sim d_{iso}^2/\alpha_{iso}$. After t_{+iso} has elapsed, the surface temperature corresponds to the portion ΔT_{iso} of the total temperature rise ΔT_∞. To first approximation the overall time constant can be written as

$$t_+ \approx t_{+iso} + \frac{(\Delta T_\infty - \Delta T_{iso})}{\Delta T_\infty} t_{+sub}, \tag{5}$$

where $t_{+sub} \approx 4 d_{sub}^2/(\pi^2 \alpha_{sub})$ is the rise time of the substrate without the insulation layer. Equation (5) states that time constant t_{+sub} of the substrate contributes to t_+ only in as much as ΔT_{sub} contributes to ΔT_∞. Since $t_{+\text{sub}}$ is typically larger than $t_{+\text{iso}}$, this can cause t_+ to be smaller than $t_{+\text{sub}}$, as shown in Fig. 5(a).

Inserting Eq. (4) into Eq. (5) yields

$$t_+ \approx \frac{4d_{\text{iso}}^2}{\pi^2 \alpha_{\text{iso}}} + \frac{1}{1+(d_{\text{iso}}/d_{\text{sub}})(k_{\text{sub}}/k_{\text{iso}})} t_{+\text{sub}} \qquad (6)$$

which reveals the functional relation between t_+ and d_{iso}. The second term in Eq. (6) dominates for small d_{iso} leading to the observed reduction in the rise times. For large values of d_{iso} the first term in Eq. (6) prevails and yields the expected quadratic behavior.

Figure 5(b) shows the rise time as a function of the substrate thickness d_{sub} for 500- and 1000-μm-wide heaters without an insulation layer. For small values of d_{sub}/w_r (in the parallel-plate limit) the rise time becomes independent of w_r and scales approximately as the square of d_{sub}, whereas for large d_{sub}/w_r the dependence is weaker. The solid curve in Fig. 5(b) labeled 1D corresponds to the rise times in the one-dimensional limit. This curve is exactly proportional to d_{sub}^2 and an excellent approximation to $t_+(d_{\text{sub}})$ for small ratios d_{sub}/w_r.

C. Feedback control—detecting the presence and location of liquids on a surface

For automated and reliable operation of microfluidic delivery devices, it is desirable to have feedback control, which determines the current location of liquid droplets and films and adjusts the surface temperature distribution to propel the liquid. For electrically conductive liquids, feedback can be provided by resistance sensors, such as pairs of electrodes which report an open circuit when no liquid is present and a finite resistance when liquid covers both. For nonconductive liquids capacitance sensors can be used.[19,20] It would be most advantageous, however, if the feedback control did not require additional electronic sensor devices but could be carried out with the heater electrodes.

The rise time t_+ is sensitive to the presence and thickness of a liquid layer on the surface. In this case the heat flux propagates in two directions and not just towards the heat sink. Fig. 6 shows the rise time as a function of the thickness of the liquid layer for three different liquids—polydimethylsiloxane (PDMS), glycerol [$C_3H_5(OH)_3$], and water—on a 500-μm-thick polyimide substrate. The material parameters of these liquids are listed in Table I.[21–28] Thermally induced convection and evaporation in the liquid layer were neglected. In each case, t_+ increases from about 0.6 s to about 0.9 s for a 100-μm-thick fluid layer. This rise-time increase can be used to monitor electronically the location and thickness of liquid droplets and films on a solid surface without the need for additional embedded or external sensor devices such as lasers and photodetectors. Measurement of the rise time t_+ can, therefore, provide a feedback mechanism for automated control of a microfluidic device based on thermocapillary transport.

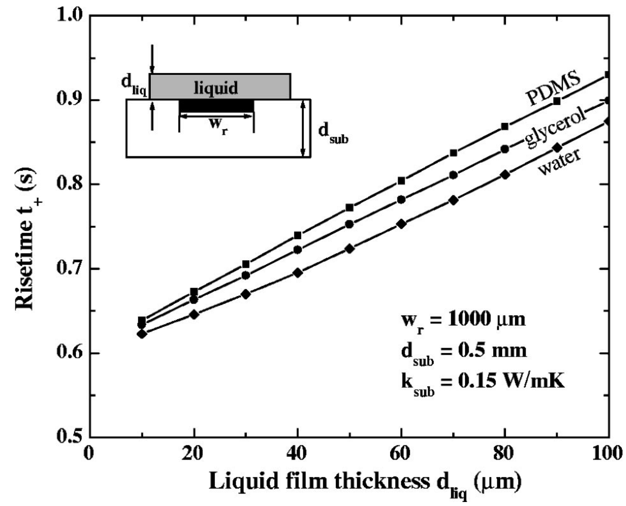

FIG. 6. Variation of rise time t_+ as a function of film thickness d_{liq} of a liquid covering the top surface of a 0.5-mm-thick polyimide substrate. t_+ increases by as much as 50% for a 100- μm-thick film compared to the case of $d_{\text{liq}}=0$. The same *relative* increase occurs for a liquid film on a glass substrate.

D. Pulsed versus continuous heating

The pulsed heating of only one resistor at a time while sequentially looping through all resistors of an array is an attractive mode of operation, because it requires only a single voltage source. The temperature of an individual heater can be controlled by modifying the number of pulses, the pulse amplitude, or pulse duration. The surface temperature can be determined via the temperature coefficient of the electrical resistivity by measuring the electrical current. However, there are some disadvantages with pulsed mode operation. It requires faster electronics and a higher peak power for the same time-averaged power value necessary to maintain a certain temperature difference ΔT. This potentially increases thermal stresses in the electrical and thermal insulation layers. In order for the temperature evolution to be acceptably smooth and continuous, the cycle or frame time τ must be much smaller than the risetime t_+.

Figure 7(a) contrasts the time evolution of the surface temperature at the center of a 500-μm-wide resistor for continuous versus pulsed heating at a frequency of 25 Hz. The thickness of the insulating polyimide layer was 25 μm. The pulse duration was half the frame time and the power was held constant during this interval. The frame time $\tau=40$ ms is approximately one fifth of rise time t_+ of about 200 ms. Nevertheless, the temperature for pulsed heating exhibits large oscillations with an amplitude A of about 3.6 K as compared to an asymptotic value ΔT_∞ of approximately 11.1 K. Figure 7(b) shows amplitude A of these oscillations as a function of pulse period τ. Unfortunately, A decreases rather slowly with decreasing frame time τ; only for $\tau \leqslant (t_+/20)$ is A smaller than 20% of ΔT_∞. Consequently, the frame times must be in the millisecond range if t_+ cannot be significantly increased without sacrificing lateral resolution. Temperature measurements with an accuracy of the order of 0.1 °C as well as feedback control would then become a demanding task. The rise time can be increased by eliminating the ther-

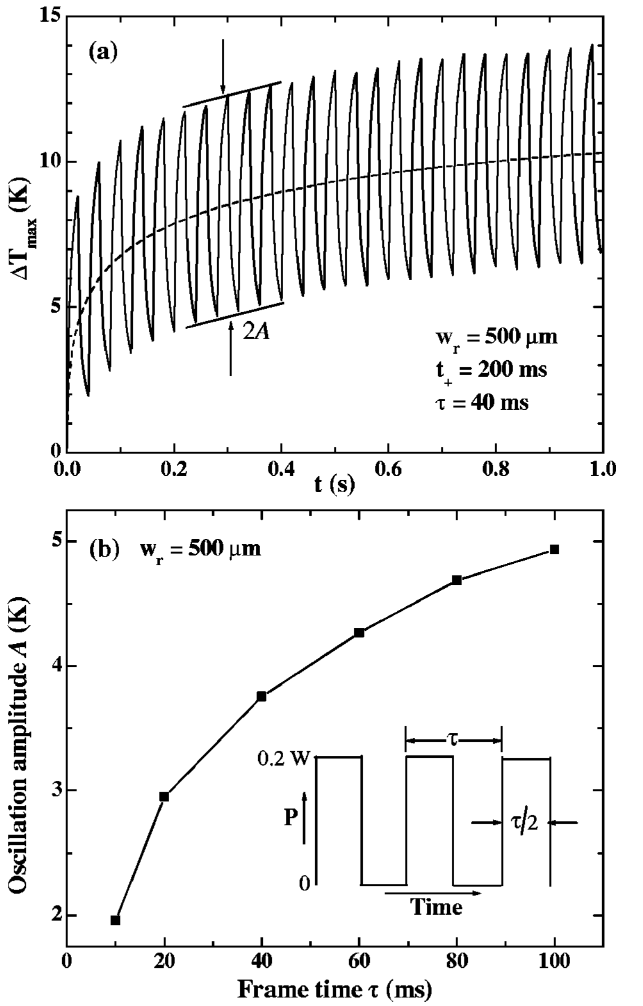

FIG. 7. (a) Evolution of the surface temperature at the center of a heater in continuous (dashed line) and pulsed heating mode (full line) for $d_{iso}=25$ μm. The frame time $\tau=40$ ms. (b) Temperature oscillation amplitude A as a function of the frame time τ for a heater width of 500 μm. Results for $w_r=1000$ μm (not shown) are $\sim$2% larger. The inset represents the pulse shape used in the simulations.

mal insulation layer or by reducing the thermal diffusivity of the substrate material, which is mainly affected by the thermal conductivity k_{sub}. Reducing k_{sub} has the additional benefit of reducing the electrical power required to maintain a desired temperature distribution.

The alternative to pulsed mode operation is continuous and simultaneous heating of all resistors in an array. This mode requires individually controllable active elements for each resistor, e.g., independent voltage or current sources or tunable resistors in series with the heating elements. For the latter case, the sensitivity of temperature measurements via the electrical resistivity change may be compromised and separate temperature sensors may be adequate. This was the approach of Sammarco and Burns.[7] Continuous heating provides smooth temperature evolutions and does not require fast control electronics. In addition, the reduction of the thermal response times for an insulation layer thickness between 25 and 100 μm can be exploited to minimize the device response time.

IV. SUMMARY

We have performed numerical heat transfer calculations to study the generation of high spatial resolution temperature distributions along a solid surface. The proposed setup consists of a thin substrate with embedded subsurface heating elements on a temperature-controlled metal block, which acts as a heat sink. The achievable lateral resolution of the temperature profile is approximately equal to the substrate thickness. The power consumption is inversely proportional to the substrate thickness and can be reduced by deposition of a thermal insulation layer in between the heating elements and the substrate.

The thermal response time t_+ of the system increases with increasing thickness of the substrate and increasing width of the heating elements and depends nonmonotonically on the thickness of the insulation layer. For pulsed-mode heating of the resistors, the pulse period must be smaller than a few percent of t_+ in order for the temperature evolution to be acceptably smooth. The rise time is sensitive to the presence and thickness of a liquid layer adhering to the top surface, which can provide a feedback mechanism for the automated control of microfluidic devices based on thermocapillary flow.

ACKNOWLEDGMENTS

This project is funded by the National Science Foundation through Grant No. CTS-0088774, a Princeton University MRSEC grant (DMR-9809483), the Molecular Level Printing Program of the Defense Advanced Research Projects Agency (DARPA), and the New Jersey Commission on Science and Technology.

[1] R. E. Cavicchi, G. E. Poirier, J. S. Suehle, M. Gaitan, S. Semancik, and D. R. Burgess, J. Vac. Sci. Technol. A **12**, 2549 (1994).
[2] R. E. Cavicchi, J. S. Suehle, K. G. Kreider, B. L. Shomaker, J. A. Small, M. Gaitan, and P. Chaparala, Appl. Phys. Lett. **66**, 812 (1995).
[3] Z. Tang, S. K. Fung, D. T. Wong, P. C. Chan, J. K. Sin, and P. W. Cheung, Sens. Actuators B **46**, 174 (1998).
[4] S. K. Fung, Z. Tang, P. C. Chan, J. K. Sin, and P. W. Cheung, Sens. Actuators A **54**, 482 (1996).
[5] K. Akahori, E. Shinohara, K. Tashiro, and S. Shoji, in *Micro Total Analysis Systems 2000*, edited by A. van den Berg (Kluwer Academic, (Dordrecht, 2000), p. 493.
[6] T. Kajiyama, K. Murakawa, and Y. Miyahara, in *Micro Total Analysis Systems 2000*, edited by A. van den Berg (Kluwer Academic, (Dordrecht, 2000), p. 505.
[7] T. S. Sammarco and M. A. Burns, AIChE J. **45**, 350 (1999).
[8] T. S. Sammarco and M. A. Burns, J. Micromech. Microeng. **10**, 42 (2000).
[9] V. Ludviksson and E. N. Lightfoot, AIChE J. **17**, 1166 (1971).
[10] A. M. Cazabat, F. Heslot, S. M. Troian, and P. Carles, Nature (London) **346**, 824 (1990).
[11] M. K. Smith, J. Fluid Mech. **294**, 209 (1995).
[12] D. E. Kataoka and S. M. Troian, Nature (London) **402**, 794 (1999).
[13] A. A. Darhuber, S. M. Troian, and W. W. Reisner, Phys. Rev. E **64**, 031603 (2001).
[14] J. P. Holman, *Heat Transfer* (McGraw-Hill, New York, 1997).
[15] J. R. Welty, C. E. Wicks, and R. E. Wilson, *Fundamentals of Momentum, Heat and Mass Transfer* (Wiley, New York, 1984). The value of $h=7.5$ W/m^2 K corresponds to heat loss by natural convection above a horizontal plate for a characteristic sample dimension $L=2.5$ cm and a temperature difference $\Delta T\approx 20$ K between plate surface and T_{amb}.
[16] H. S. Carslaw and J. C. Jaeger, *Conduction of Heat in Solids* (Oxford University Press, Oxford, U.K., 1959).

[17] A. A. Darhuber, J. M. Davis, W. W. Reisner, and S. M. Troian, *Proceedings of Micro Total Analysis Systems 2001*, edited by J. M. Ramsey and A. van den Berg (Kluwer Academic, Dordrecht 2001), p. 244.
[18] S. Wolf and R. N. Tauber, *Silicon Processing for the VLSI Era* (Lattice, Sunset Beach, CA, 1987).
[19] K. J. Elkow and K. S. Rezkallah, Int. J. Multiphase Flow **23**, 815 (1997).
[20] T. Merkel, L. Pagel, and H.-W. Glock, Sens. Actuators A **80**, 1 (2000).
[21] 1737F Material Information, Corning Advanced Display Products.
[22] Durimide Material Information, Arch Chemicals, Norwalk (2000).
[23] Kapton Product Information Sheets, DuPont High Performance Films, Circleville (1997).
[24] Pyralin Product Information, HDMicroSystems, Wilmington (2000).
[25] *Handbook of Chemistry and Physics* (CRC, Boca Raton, FL, 1982).
[26] M. Firon, M. C. Hugon, B. Agius, Y. Z. Hu, Y. Wang, and E. A. Irene, J. Vac. Sci. Technol. B **14**, 2543 (1996).
[27] *Electrical Resistivity Handbook*, edited by G. T. Dyos and T. Farrell (Peregrinus, London, U.K., 1992).
[28] Silicone Fluids Property Profile Guide, Gelest, Inc. (1998).